

**Proposal to Measure $\Delta\sigma^{\gamma N}(k)$ and the High
Energy Contribution to the Gerasimov-Drell-Hearn Sum Rule**

V. Ghazikhanian, G. Igo, S. Trentalange
University of California Los Angeles, Los Angeles CA 90095

N. Bianchi, V. Muccifora
INFN Laboratori Nazionali di Frascati, I-00044, Frascati, Italy

S. Bueltmann, Jian-Ping Chen, J. Mitchell
Jefferson Lab, Newport News VA 23606

G. Court
University of Liverpool, Liverpool L69 3BX, United Kingdom

R. G. Arnold, P. E. Bosted(*), R. Hicks, R. Miskimen,
G. Peterson, S. E. Rock, J. Shaw
University of Massachusetts, Amherst, Massachusetts 01003 (*) co-spokesperson (contact:
Bosted@Slac.Stanford.Edu)

R. Lombard
*DAPNIA-Service de Physique Nucleaire Centre d'Etudes de Saclay, F-91191 Gif/Yvette,
France*

G. Tamas
Institut fur Kernphysik, D55099 Mainz, Germany

G. Mitchell, S. Penttila
Los Alamos National Laboratory, Los Alamos, New Mexico 87545

A. Klein, S. Kuhn, C. Hyde-Wright
Old Dominion University, Norfolk, Virginia 23529

St. Goertz, W. Meyer, G. Reicherz
Ruhr-UniversitBochum, Universitstr 150, Bochum, Germany

P. Decowski
Smith College, Northampton, Massachusetts 01063

P. Anthony, R. Erickson, T. Fieguth, S. Rokni,

S. St.Lorant, Z. M. Szalata, D. Walz, M. Woods
Stanford Linear Accelerator Center, Stanford, California 94309

D. Crabb(*), D. Day,
R. Lindgren, D. Pocanic, O. Rondon, F. Wesselmann
University of Virginia, Charlottesville, Virginia 22901 (*) co-spokesperson (contact:
Dgc3q@Virginia.Edu (804) 924-6790)

D. Armstrong, T. Averett, K. Griffioen
College of William and Mary, Williamsburg, Virginia 23187

N. Akopov, A. Apyan, R. Avakian, A. Avetisian,
S. Darbinian, K. Ispirian, S. Taroyan
Yerevan Physics Institute, Yerevan, Armenia

Abstract

We propose to measure the spin-dependent total cross section for circularly polarized photons absorbed on longitudinally polarized protons and neutrons in the photon energy range $5 < k < 40$ GeV. This will be the first measurement of the difference between left- and right-handed polarized photoproduction above the resonance region. These data are needed to learn about the high energy convergence of the fundamental Gerasimov-Drell-Hearn sum rule for the proton and neutron. Substantial contributions are expected in the SLAC energy range, especially for the isovector combination. Measurements of the magnitude and energy-dependence of polarized photoabsorption at high energy will provide the baseline for understanding of soft Regge physics, essential to the interpretation of data taken with virtual photons.

The photon beam will be produced using collimated coherent bremsstrahlung from a diamond crystal. The polarized targets will use NH_3 and ND_3 to provide polarized protons and deuterons. Calorimetric detectors will be used to identify hadronic interactions and reject electromagnetic backgrounds. We request re-establishment of the coherent bremsstrahlung photon facility for End Station A, resources for the polarized targets, and two months of running time at 120 Hz with electron beam energies between 10 and 48 GeV.

1 Introduction and Motivation

1.1 The GDH Sum Rule

The Gerasimov-Drell-Hearn (GDH) sum rule [1] is one of the most fundamental relations in hadronic physics, and its experimental test is one of the major challenges for photoproduction experiments over the next decade. The GDH sum rule relates the difference in total hadronic photo-absorption cross sections for left- ($\sigma_A^{\gamma N}$) and right-handed ($\sigma_P^{\gamma N}$) circularly polarized photons interacting with longitudinally polarized nucleons to the square of the nucleon's anomalous magnetic moment κ ,

$$\int_{k_\pi}^{\infty} \frac{dk}{k} \Delta\sigma^{\gamma N}(k) = \frac{2\pi^2 \alpha \kappa^2}{M^2} \quad (1)$$

where k is the photon energy, $\Delta\sigma^{\gamma N}(k) = \sigma_P^{\gamma N}(k) - \sigma_A^{\gamma N}(k)$, M is the nucleon mass, and the threshold energy k_π needed to produce at least one pion is about 0.15 GeV. An alternate notation is $\Delta\sigma^{\gamma N} = \sigma_{3/2}^{\gamma N} - \sigma_{1/2}^{\gamma N}$, where 1/2 (3/2) refers to the spin of the nucleon-photon system. Note that we have chosen a definition of $\Delta\sigma^{\gamma N}(k)$ for which the GDH integral is positive: frequently the opposite sign convention is chosen.

Numerically, the GDH sum rule prediction is 204 μb for the proton, 232 μb for the neutron, and 219 μb (-15 μb) for the average isoscalar (isovector) combinations. The fundamental meaning of the sum rule is that any particle with a non-zero anomalous magnetic moment must have an excitation spectrum and internal structure. The energy scale at which the sum rule is saturated gives an indication of the energy scale beyond which nucleonic excitations become asymptotically spin-independent.

Many authors [2] have analyzed the connection between the GDH sum rule, valid for real photons ($Q^2 = 0$), and the analogous sum rules for virtual photons, in particular the equally fundamental Bjorken Sum Rule [3] for $Q^2 \rightarrow \infty$, which has been the subject of intense experimental study in the past decade. A generalized GDH Sum Rule can be formed that smoothly connects the $Q^2 = 0$ and large Q^2 limits. The goal of the present proposal is to augment the large body of data recently acquired at SLAC with virtual photons, with new data using real photons. This will provide valuable $Q^2 = 0$ anchor points for the study of spin-dependent photo-absorption cross sections in the 5 to 40 GeV energy range, thought to be responsible for much of the isovector sum rule strength. Because there are no existing data in this energy region, it will be an exciting experimental venture, with surprising results certainly possible. Such was the case with the $Q^2 > 0$ measurements, which have concluded that the Ellis-Jaffe sum rules for the proton (p) and neutron (n) are strongly violated, although the more fundamental isovector ($p - n$) Bjorken Sum Rule rule has been validated within experimental errors. Data from this proposal will compliment the vast body of spin-averaged data on $\sigma^{\gamma N}(k)$. Measurements of the spin degree of freedom will help to gain insight into underlying reaction mechanism for photo-absorption, such as the role of reggeon exchange and a possible pomeron cut contribution. A good understanding of soft Regge physics is essential for the interpretation of the Q^2 -dependence of data taken with virtual photons.

1.2 Energy Dependence of $\Delta\sigma^{\gamma N}$

Based on the $1/k$ factor in the GDH integral, combined with the expectation of a strong spin dependence in the excitation of the dominant nucleon resonances (for example, $\sigma_{1/2}^{\gamma N} \approx (1/3)\sigma_{3/2}^{\gamma N}$ for the prominent $\Delta(1232)$ resonance), one would guess that the GDH integral would be saturated at photon energies of about 1.7 GeV, the traditional cutoff between the resonance region and deep inelastic scattering. Multipole analyses [4] of unpolarized pion photoproduction data suggest that for the proton or neutron individually, the resonance region contributions are about 20% above (for the proton) or below (for the neutron) the sum rule values, with substantial contributions possible at higher energies. In the isovector case (difference of proton and neutron), the contributions from major resonances such as the $\Delta(1236)$ cancel, with principally *non-resonant* contributions at low energy, and equally large contributions at high energy.

As summarized by [5], the resonance region multipole analyses give integral values of 257 to 289 μb for the proton (well above the GDH integral), and 169 to 189 μb for the neutron (well below the GDH integral). Looked at another way, the resonance region would seem to account for most of the *isoscalar* $[(p+n)/2]$ strength, but gives contributions of 34 to 65 μb for the *isovector* $[(p-n)/2]$ combination, compared to the GDH value of -15 μb . We can therefore deduce that the integrated strength above the resonance region should be quite large (of order 25 to 50 μb) for both proton and neutron, but of opposite sign.

The multipole analyses have several drawbacks, one of the most important being that not all channels are considered. For reliable determinations of $\Delta\sigma^{\gamma N}$, it is essential to make direct measurements of the total cross section difference using polarized photons and polarized targets. An experimental program to accomplish this is currently underway at beam energies up to 3 GeV. The interesting experimental question is how high above the resonance region one must go to saturate the missing strength. The energy region of 5 to 40 GeV accessible at SLAC extends the upper limit of integration by about an order of magnitude, which will likely be high enough if $\Delta\sigma^{\gamma N}$ is smoothly decreasing in strength with increasing energy. However, as in the resonance region, specific degrees of freedom for nucleon excitations can come in to play to cause oscillations in the magnitude of $\Delta\sigma^{\gamma N}$ which may well be significant. As an example, the SLAC energy range spans charm threshold. It is entirely possible that $\Delta\sigma^{\gamma N}$ is approximately constant in the SLAC energy range, which would imply that excitations at even higher energies play a crucial role in preventing the GDH integral from becoming divergent.

Regge theory gives a good description of many processes, and thus should be a reasonable guide to the high energy behavior of $\Delta\sigma^{\gamma N}$. In this framework, the energy dependence for a given Regge trajectory is given by s^{α_0-1} , where $s = M^2 + 2Mk$ is the squared total center of mass energy, and α_0 is the intercept, which is related to the spin J , mass m_r , and intercept slope α' (of order $0.8 - 0.9 \text{ GeV}^{-2}$) by $\alpha^0 = J - \alpha' m_r^2$. As discussed in some detail in [5, 6], the isovector contribution to $\Delta\sigma^{\gamma N}$ is expected to be dominated by the poorly known $a_1(1260)$ axial vector meson trajectory (α^0 is generally thought to be in the range -0.5 to 0), while the isoscalar contributions are expected to be dominated by the better known $f_1(1285)$ meson trajectory (α^0 of -0.4 ± 0.1). Contributions from higher mass

trajectories could also be important. In addition, both [6] and [5] consider possible isoscalar contributions from non-perturbative gluon exchange (proportional to $\ln s/s$) as suggested by [7]. Finally, [6] also considers a possible two-pomeron cut contribution (proportional to $1/\ln s^2$). The shape of each of these four contributions with the parameters chosen by [6] is shown in Fig. 1 as a function of photon energy. The strength of each curve was normalized as in [6] to a value of about $-20 \mu\text{b}$ at $k = 5 \text{ GeV}$. Three predictions from [5] are also shown in Fig. 1.

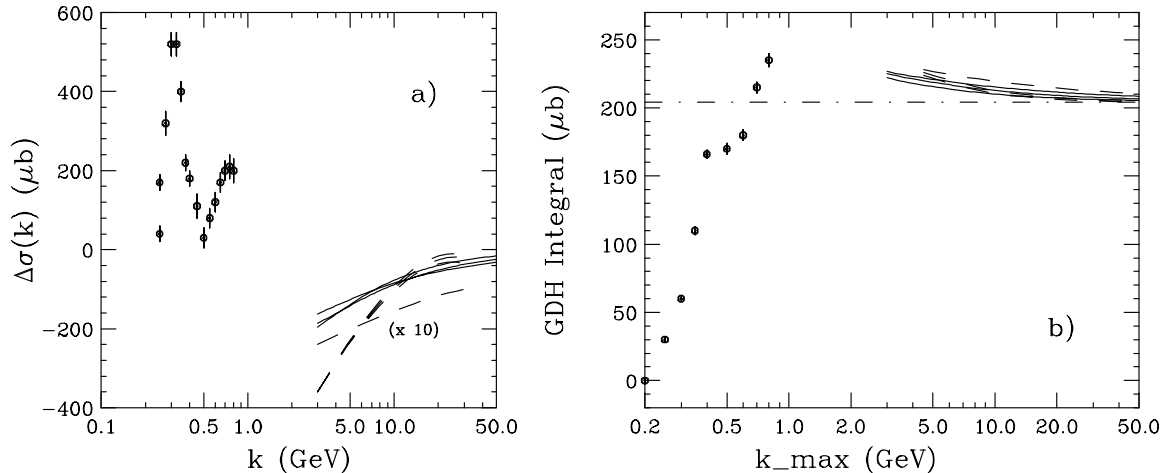


Figure 1: a) Very preliminary data for $\Delta\sigma^{\gamma N}(k)$ for the proton from MAMI [8] along with possible extensions to higher energy from [6] (dashed curves) and [5] (solid curves), scaled by a factor of 10; b) same but for the GDH integral as a function of the upper limit of integration. Theory curves are plotted assuming the sum rule converges at 1 TeV. The dot-dashed line is the asymptotic prediction.

1.3 Connection to Virtual Photo-absorption

Bianchi and Thomas [5] have shown that extending their Regge parameterization to $Q^2 > 0$ can give a quite reasonable description of all available deep inelastic data for the spin structure function g_1 , covering a wide range of x and Q^2 . They made three different fits, with slight variations in some of the assumptions, and all of them give a $\chi^2/\text{d.f.}$ as good as NLO pQCD fits based on polarized quark and gluon distribution functions. This shows the duality between different ways of describing hadronic physics. From our point of view, the big advantage of the Regge theory is that it allows a prediction of $\Delta\sigma^{\gamma N}(k)$ for real photons. From another point of view, good measurements with real photons might help to understand the high energy (low- x) behavior of g_1 , especially if the $(\ln s)/s$ or pomeron-pomeron cut contributions are larger than expected [6]. The existing data for g_1 are shown in Fig. 2, along with one of the Regge fits, and an NLO pQCD fit. It can be seen that there is a considerable uncertainty in extrapolating the data on g_1 to $x = 0$. This is currently the largest uncertainty in testing the Bjorken and Ellis-Jaffe sum rules, which both involve

integrals of g_1 over the range $0 < x < 1$. Especially in the neutron case, the $\chi^2/\text{d.f.}$ for fits that give a divergent integral are only slightly worse than fits that give a convergent integral. It will be very interesting to measure the analogous cross sections with real photons.

1.4 Experimental status

The resonance region contributions up to about $k = 3$ GeV are presently being measured at LEGS, MAMI, GRAAL, and ELSA, with an extension to 6 GeV possible at Jefferson Lab [8]. Very nice measurements up to 800 MeV have recently been completed at MAMI (see Fig. 1), and are currently underway at ELSA up to 3 GeV. Unfortunately, the measurements are only for polarized protons at present. Preliminary indications are that the proton sum rule is already exceeded at 800 MeV (Fig. 1b), implying that $\Delta\sigma^{\gamma N}(k)$ should change sign at some higher energy, as predicted by the fits of [5, 6], shown in Fig. 1a scaled by a factor of 10. Threshold contributions may reduce the integral shown in Fig. 1b by a small amount, but this does not alter the conclusion that $\Delta\sigma^{\gamma N}(k)$ should change sign above 800 MeV.

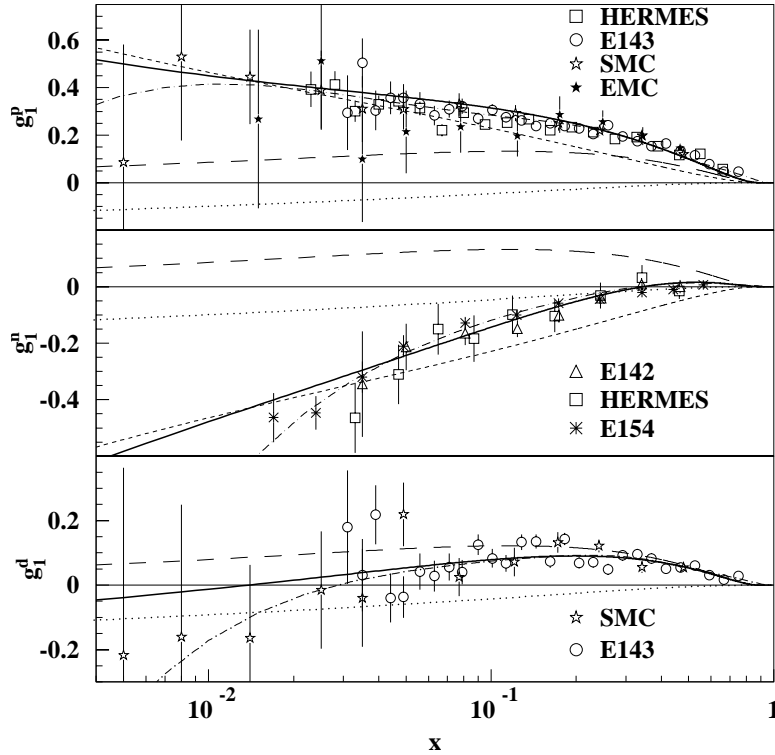


Figure 2: The solid curves are the Model II Regge fit of [5] compared to world data on g_1 at $Q^2 = 3$ GeV². The short dashed, long dashed, and dotted curves represent the a_1 , f_1 , and two-gluon contributions, respectively. The dot-dashed curve is an NLO pQCD fit. Taken from Fig. 3 of [5].

To fully test the GDH sum rule, the high energy behavior must be determined for both proton and neutron targets, in order to test the isoscalar and isovector sum rules

separately. SLAC is presently the only lab where measurements for $k > 6$ GeV can be made. Measurements up to at least 30 or 40 GeV are essential to understand how the sum rules for both the proton and neutron are converging, and to make the connection to the extensive body of data taken with virtual photons.

1.5 How to measure $\Delta\sigma^{\gamma N}(k)$ for the neutron

We plan to measure $\Delta\sigma^{\gamma N}(k)$ for the neutron by using both proton and deuteron targets, and making small corrections to the approximation that the deuteron is the average of proton and neutron cross sections. As we did for virtual photons, we will take into account the approximately 5% D-state probability in the deuteron wave function. At very low energies there are corrections due to processes such as deuteron photodisintegration near threshold (2.2 MeV) and coherent π^0 production, as well as effects due to final state interactions, meson exchange currents, shadowing, and relativistic effects [9]. We expect these effects to be small at SLAC energies, on the order of a few percent (comparable to the size of experimental systematic errors).

It is possible to study this assumption by comparing $\Delta\sigma^{\gamma n}(k)$ extracted from both polarized deuterium and ^3He . About 87% of the ^3He wave function is a polarized neutron with a pair of unpolarized protons [10]. Since nuclear corrections are quite different for ^3He and deuterium, comparing the results extracted for the neutron can give valuable constraints on the systematic errors involved in the extraction.

2 Experimental Overview

The experimental setup has been optimized to meet the beam conditions available in End Station A at SLAC, in particular the duty cycle of $< 10^{-4}$. An effort has been made to make optimal use of the equipment for the present E158 experiment.

We will use an untaged coherent bremsstrahlung beam to create a high flux of circularly polarized photons (section 3.1). With coherent bremsstrahlung, a set of high intensity spikes is generated by proper orientation of a diamond crystal radiator. A low-Z beam hardener is used to reduce the intensity of photons below 100 MeV. A collimator is used to enhance the ratio of coherent to incoherent radiation. For photon energies up to about 30 GeV, a substantial fraction of the measured $\Delta\sigma^{\gamma N}(k)$ will come from the primary intensity spike. The contributions from low energy, incoherent photons will be measured using an amorphous carbon radiator. A simultaneous fit to all the measurements will produce a best fit for $\Delta\sigma^{\gamma N}$ as a function of k .

For targets, we will use polarized NH_3 and ND_3 as sources of polarized protons and neutrons (section 4). Polarized deuterons to first order allow measurements of the isovector combination $(n + p)/2$, with small corrections for the deuteron D -state, shadowing, and nuclear coherent hadron production. An extension to this proposal could use a polarized ^3He target to verify the consistency of $\Delta\sigma^{\gamma n}(k)$ for the neutron as extracted from either deuterium or ^3He . The detector is optimized to measure $> 98\%$ of all hadronic interactions, and to reject electromagnetic backgrounds.

We envision taking data in two modes: counting mode and flux integration mode. In the counting mode, all particles except neutrinos emerging from the target with sufficient energy and angle $\theta_{min} < \theta < \theta_{max}$ are counted in one of two total absorption lead/scintillator calorimeters, with each segmented longitudinally for electromagnetic showers (first 27 r.l.) and hadronic showers (remaining 53 r.l.). A hadronic interaction is identified with very high efficiency using suitable kinematic cuts that reduce the electromagnetic background to a small level. The target geometry fixes θ_{max} at 20 degrees, while the movable detector geometry determines $\theta_{min} = 0.01\sqrt{40/k_0}$ as an optimal tradeoff between signal and background. Approximately five hadronic interactions originating from coherent photons will be detected per beam spill in the counting mode.

Using the counting mode, we can verify the reasonable assumptions that the energy per event in the hadronic part of the calorimeter is independent of photon helicity, and that the total energy from electromagnetic background events is negligible. If these assumptions are verified, we can obtain significantly smaller statistical errors by raising the beam current to a level corresponding to several hundred nuclear interactions per beam spill, and simply measure the asymmetry in the total energy deposition in the hadronic part of the calorimeter. As a further systematic check, we can also integrate the energy in both the electromagnetic and hadronic portions of the detector, and use calculations to account for the rate and asymmetry of the electromagnetic processes. This method has the advantage of minimizing the sensitivity to a possible helicity-dependence to the fractional energy into π^0 's.

We plan to extract $\Delta\sigma^{\gamma N}$ from the data in two ways. In the first method, the difference of rates for the two helicity states is converted to cross sections directly using the measured detector acceptance and target thickness. In the second method, the asymmetry in counting rates will be corrected by a calculated dilution factor, and converted to $\Delta\sigma^{\gamma N}$ using previously measured values of $\sigma^{\gamma N}(k)$. In this method, factors such as the detector efficiency cancel, so that some systematic errors will be reduced (while others will be increased). The expected magnitude of the experimental asymmetries is relatively small, and will likely be less than 0.01 at the lowest photon beam energy, and a factor of 10 to 100 smaller at higher energies. Comparison of the two analysis methods will give a valuable check on the evaluation of systematic errors.

Details of the photon beam, target, detector, and expected experimental sensitivity are given in the next sections. The last section summarizes our request for beam time and equipment.

3 Photon Beam

3.1 Choice of Beam Type

Because the total cross section is known to be approximately constant at about 120 μb for $5 < k < 40$ GeV, and the asymmetry is expected to decrease with increasing energy, it is strongly preferable to have a nearly monochromatic photon beam to perform this experiment. A tagged photon beam was used in the SLAC experiment that measured

the total cross section [12], but due to the poor duty factor at SLAC this method would not provide enough intensity to measure $\Delta\sigma^{\gamma N}(k)$ with the desired accuracy. Untagged Compton backscattering with small angle collimation could in principle provide a nearly monochromatic polarized beam, but detailed studies have shown that sufficient intensities cannot be obtained in End Station A at high energies due to synchrotron radiation induced emittance growth. Sufficient intensity could possibly be obtained in the FFTB area, but only if a short pulse (< 1 ns) damped beam were to be used, which would allow running only in the flux integration mode, without the systematic checks afforded by the counting mode. The FFTB area would also require major investment in new equipment to provide the $10 \mu\text{r}$ collimation angle needed to make the photon beam nearly monochromatic.

Fortunately, a collimated coherent bremsstrahlung photon beam can provide a quasi-monochromatic, highly polarized photon beam of sufficient intensity. This technique was successfully used in a previous SLAC experiment [13]. A schematic layout of the photon beam line is shown in Fig. 3. The polarized photon beam is produced using bremsstrahlung from 9.9 to 48.5 GeV longitudinally polarized electron beams transported through the SLAC A-line. The beam energies will be multiples of 3.237 GeV to preserve longitudinal polarization (with small adjustments at high energy to account for synchrotron radiation). We assume an electron beam with characteristics similar to those obtained for the recent spin structure function experiments SLAC E154 and E155: an intensity of up to 1×10^{11} electrons per pulse; repetition rate of 120 Hz; pulse length of 500 nsec; and polarization of about 83%.

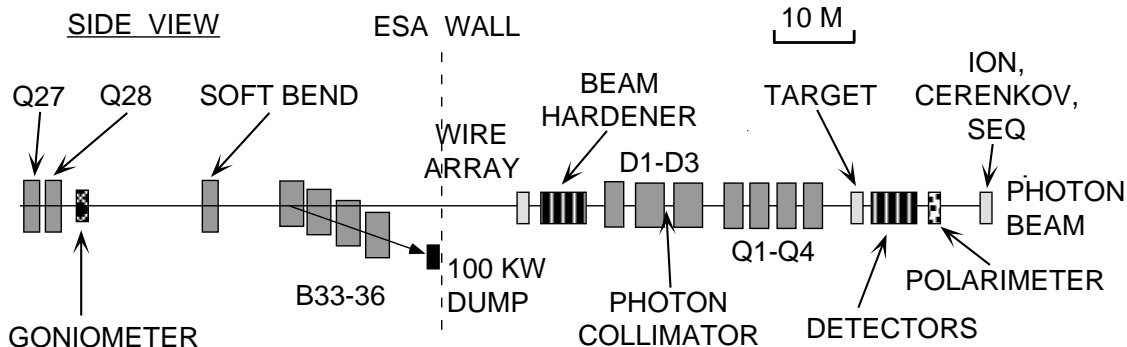


Figure 3: Overall view of the main components of the photon beam (horizontal scale is approximate, vertical scale is exaggerated). The Wire Array, D1-D3 dipole magnets, and Q1-Q4 quadrupoles are part of the current E158 setup. The Beam Hardener is at the E158 LH2 target location.

For most of the running, the electrons will be incident on a 0.0007 radiation length (r.l.) thick oriented diamond crystal with a tilt angle θ_0 of a few milliradians. The 0.0007 r.l. thickness is a good compromise between photon flux and coherent peak width, which increases for thicker radiators due to multiple scattering of the primary electron beam. The diamond will be positioned using the SLAC goniometer [14], which can hold two radiators, and position either of them at well-defined angles with respect to the beam axis, in steps of

25 μ r. The goniometer will be located just downstream of the Q27/Q28 quad pair at the end of the A-line, as in SLAC E78 [13].

Based on previous experience, it may be necessary to change crystals once or twice during the experiment, due to radiation damage to the lattice. This will be determined by monitoring the height of the coherent peaks.

The A-line quadrupoles will be adjusted to give a beam spot size of at least 10 mm² at the diamond to avoid overheating. The quadrupoles will also be adjusted to give a small waist at the position of the collimator. For energies below 35 GeV, it is possible to obtain spot sizes smaller than 0.7 mm by 0.7 mm. At 48 GeV, the beam will be wider in the horizontal (about 1.5 mm) due to the increased energy spread from synchrotron radiation in the A-line, which grows at the fifth power of beam energy. We have verified that the desired optics can be obtained without quadrupoles Q30 and Q38, which are located down-beam the goniometer and not used in this experiment.

Tuning of the electron beam will be done by sending the beam at low repetition rate (10 Hz or less) and low current into End Station A and using the beam position monitors, screens, and wire array built for E158.

To obtain photon beams, the electrons will be bent into a dump using the existing B33-36 dipole magnets. Just upstream of B33, we plan to place a weak magnet with a total field strength of 0.1 kG-m. This bends 48.5 GeV electrons by 0.2 mr. The purpose of the initial soft bend is to minimize the number of energetic synchrotron radiation photons impinging upon the target 110 m downstream. The B33-B36 dipoles are not strong enough to bend electrons with $E > 25$ GeV into the existing high power dump. Therefore we will move the magnets to accommodate a smaller bend angle, and use a 50 kW dump for the electrons, positioned downstream of and below the Q38 quadrupole. This will require modifying the vacuum chambers of the magnets. Although we do not plan to run higher than 20 kW, a 50 kW dump will allow some flexibility for tests or other experiments.

After entering the End Station, the photon beam first passes through a 3 r.l. carbon beam hardener at the location of the E158 target. The hardener attenuates photons above 100 MeV by an approximately constant factor, but has much larger attenuation for lower energy photons. This reduces the low energy backgrounds in the detector by approximately a factor of five.

After the hardener, the beam passes through a variable diameter, 70 r.l. tungsten collimator to limit the transverse position and angle of the photons. Two diameters are needed: 1 mm and 3 mm, for electron beam energies of 20 to 48 GeV, and 10 to 25 GeV respectively. The corresponding collimation angles provide an optimal tradeoff between photon flux and the ratio of coherent to incoherent bremsstrahlung. About 50% to 95% of the photons will hit the collimator (depending on energy), corresponding to a maximum power into the collimator of 40 W for the 0.0007 r.l. diamond radiator. A four-quadrant, tungsten pin-cushion shower-emission detector as used in E78 [15] will be placed just in front of the collimator, and the beam will be centered by matching the signals in the left/right and up/down pairs.

Assuming that the existing E158 setup is in place, we plan to locate the collimator between the D2 and D3 magnets, just downstream of the 3DC3 water-cooled photon col-

limator (inner radius 8 mm). The E158 D3 dipole magnet will be powered to provide a sweeping field of 36 kG-m. This magnet will sweep charged particles produced in the collimator by an angle of at least 30 mr. A thick lead wall just in front of the target, with a 1 cm hole for the photon beam, will be used to absorb charged and neutral particles not already absorbed by quadrupoles Q1-Q4.

The photon beam, after passing through the target and an evacuated beam pipe through the spectrometer and detectors, will be finally stopped in a Secondary Emission Quantometer (SEQ), used to measure the total photon beam intensity (intensity is energy-weighted flux). Just upstream of the SEQ we will use two auxiliary detectors to monitor the beam flux: an ionization chamber and an atmospheric gas Čerenkov detector. All of these devices will be similar to those used in E78.

As in E78, the goniometer angles will be calibrated by mapping out the ratio of flux (number of photons) compared to intensity (energy-weighted flux) as a function of horizontal and vertical angles. Maxima in the ion chamber to SEQ ratios occur at well-defined settings due to channeling radiation, and can be used to determine the correct orientation of the crystal for the desired experimental settings [16]. Final tuning will be done using the Compton polarimeter described below.

3.2 Calculations of Photon Beam Flux and Polarization

We have calculated the photon beam flux and intensity profile using the formulas given in Eq. 35 of Ref. [17], as implemented in a Monte Carlo simulation following the very clear introduction to the practicalities of coherent bremsstrahlung given in [18]. As in [13], we will use crystal orientations that give a primary coherent spike at the (022) reciprocal lattice spacing, with lower intensity, higher energy spikes at (044), (066), etc. For each electron beam energy, we adjust the goniometer angle θ_0 such that the discontinuity (spike) of the lowest energy coherent peak is at a value of k_0/E between 0.5 and 0.8. With no collimation, there is a long tail extending to lower energies. This tail is mostly removed by the collimator, as originally proposed in Ref. [19]. The incoherent tail is also reduced by collimation, but in this case the reduction is independent of photon energy. A Monte Carlo program was used to fold in the effects of multiple scattering in the radiator, beam emittance, crystal mosaic spread, and beam spot size as a function of energy. The code was checked against spectra measured in [13], and gives very good agreement with these data. The intensity spectra for four representative photon spectra are shown in Fig. 4. The incoherent contribution is shown as the dashed line. The corresponding electron beam current, collimator size, and other parameters used to generate these spectra are shown in Table I. By using different collimator sizes for the different energies, a balance can be struck between sharpness of the coherent peaks, and the electron beam current needed for sufficient intensity. In addition to the main spike, smaller spikes at higher energies are present in a well-defined intensity ratio.

As will be seen below, the error on $\Delta\sigma^{\gamma N}(k)$ depends on both the average coherent photon polarization and the ratio of coherent to incoherent radiation. An increase in the former results in a decrease in the latter, and vice versa. A good way to check systematics

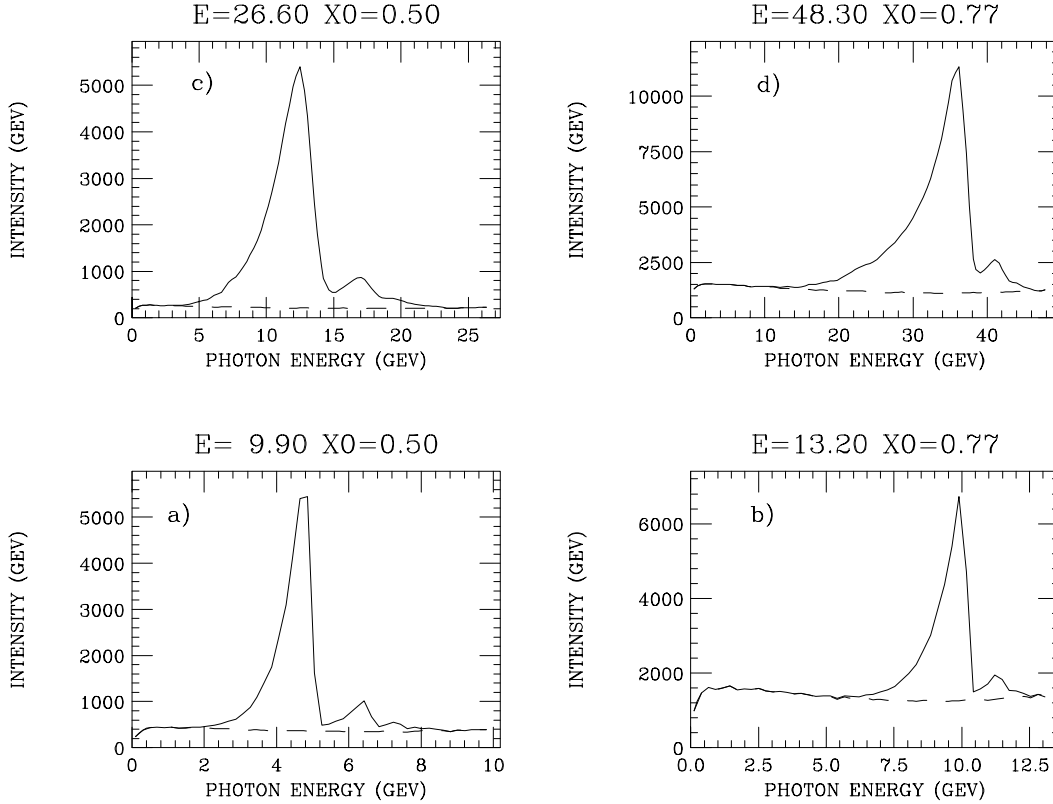


Figure 4: Calculated intensity (flux times energy) for collimated coherent bremsstrahlung at four settings as detailed in Table I. The dashed lines are incoherent radiation only, while the solid lines include coherent contributions.

is to run with similar coherent peak energies but two different endpoint energies. This is illustrated in cases b) and c) in Fig. 4.

The circular polarization of bremsstrahlung from crystals has been calculated in Ref. [20], and in the reasonable approximation that the two ψ_2 terms are equal to the corresponding coherent and incoherent ψ_1 terms, is simply given by

$$P_\gamma = P_e \frac{1 - (1 - y)^2 - \frac{2}{3}y(1 - y)}{1 + (1 - y)^2 - \frac{2}{3}(1 - y)} = P_e \frac{y(4 - y)}{4 - 4y + 3y^2},$$

where $y = k/E$. In this approximation, the polarization is the same for the coherent and incoherent components. The results of the full calculation (no approximations) are shown in Fig. 5 for two of the spectra of Fig. 4, and are almost indistinguishable from the formula given above, except for some small wiggles near the coherent intensity spikes. It can be seen that the average circular polarization increases strongly with k/E . The average coherent value for the four cases of Fig. 4 is given in Table I.

There is a linear polarization component of the coherent spikes which is independent of electron helicity, and will thus cancel when taking the difference in cross sections for the two electron spin directions. There will also be no net effect on the total cross section,

Electron Energy (GeV)	9.9	13.2	26.6	48.3
k_0/E of Main Coherent Peak	0.50	0.77	0.50	0.77
Incident Electrons/spill	5×10^9	8×10^9	1.5×10^9	2×10^9
collimator Radius (mm)	3	3	1	1
Total photons/spill	1.5×10^5	3.0×10^5	5×10^4	1.1×10^5
Coherent NI/spill	6.8	3.2	3.7	2.7
Coherent $\langle P_\gamma/P_e \rangle$	0.59	0.87	0.57	0.82
r with energy cut	0.59	0.31	0.80	0.58
$\delta\Delta\sigma^{\gamma p}$ (μb)	0.5	0.7	0.6	0.6

Table 1: Parameters related to the four representative photon spectra shown in Fig. 4, assuming a 0.0007 r.l. thick diamond radiator and a 3 r.l. Be beam hardener. Nuclear Interactions are abbreviated as NI, and r is the fraction of all detected NI coming from coherent radiation. $\delta\Delta\sigma^{\gamma p}$ is the expected statistical proton error for 10^7 beam spills (one day at 120 Hz) using the counting mode and the NH_3 target.

because of the azimuthal symmetry of our detectors. The linear polarization is between 0.1 and 0.4, depending on the choice of crystal orientation and value of k_0/E .

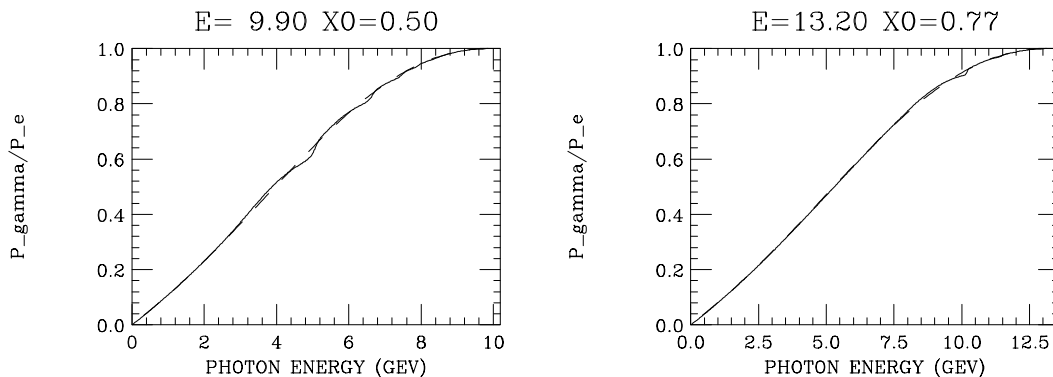


Figure 5: Photon circular polarization (relative to electron polarization) as a function of photon energy for the spectra of Fig. 4a,b. The dashed lines are for incoherent radiation while the solid lines include the coherent peaks.

3.3 Measurements of Photon Beam Flux and Polarization

We propose to measure the photon flux and polarization as a function of energy using atomic Compton scattering. This is accomplished by detecting both the scattered photon and recoil electron in coincidence. The setup will be similar to the double arm Møller setup successfully used in E143 and E155 to measure the electron beam polarization, at counting rates similar to the present proposal. For dedicated measurements, a 0.25 gm/cm^2 (0.02 r.l.) iron target will be placed in the polarized target solenoid, providing a well-defined source of polarized atomic electrons (1 in 13 is longitudinally polarized). During normal

running, the electrons in the ammonia targets will be used to monitor the energy profile. If the microwaves used for dynamic nuclear polarization are turned off, the free electrons are highly polarized, and can also be used for relative beam polarization measurements.

The layout of the Compton polarimeter is shown in Fig. 6. A 1-m-long 18D36 magnet with an integrated field of up to 15 kG-m will be placed downstream of the Small- θ calorimeter (see below for details). Both this detector and the magnet will be mounted on rails, so that the maximum angle for the Compton polarimeter can be matched to the desired energy range to be measured. We plan to measure Compton pairs in the upper half of the photon energy range, corresponding to a desirable θ_{max} of 30 mr for a 10 GeV endpoint energy, decreasing to 10 mr for 48 GeV electron beam energy. The central downstream hole in the main detector will define this θ_{max} angle. Following the magnet will be a small array of scintillators and lead glass blocks, with a ± 3 cm gap in the horizontal plane to exclude the large flux of small-angle Bethe-Heitler pairs. The top and bottom half of the detector array will each be 9 cm tall by 30 cm wide, and will be made from thirty 3x3 cm lead glass blocks. Ten scintillator paddles (each 3 cm wide) will be mounted in front of the lead glass.

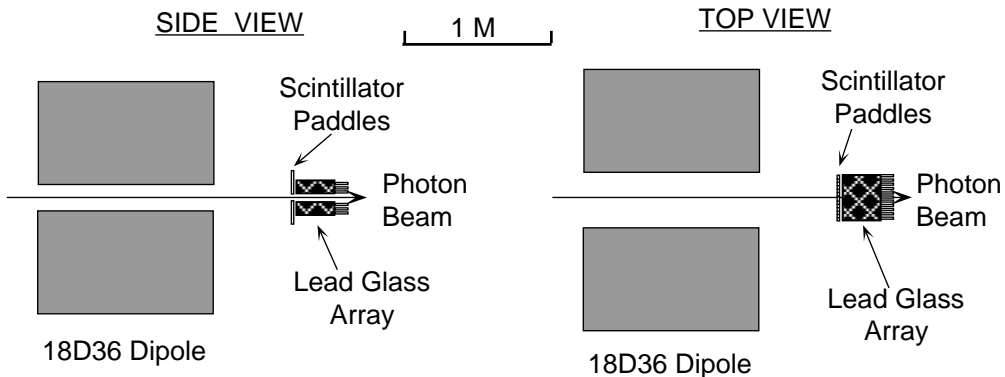


Figure 6: Layout of the magnet and detectors for the Compton polarimeter.

The total energy of the primary photon is measured as the sum of the energies of the scattered photon and recoil electron, with typical resolution of 3% to 5%. Scattered photons are separated from electrons using a veto of the front scintillators. Additional information is provided by co-planarity and invariant mass cuts. Since the atomic Compton signal dominates the detector rates, these cuts will provide a very clear Compton signal with very little background.

We have calculated rates and sensitivity to photon polarization using [21]

$$\frac{d\sigma}{d\Omega} = \frac{\alpha^2}{2m_e^2} \left(\frac{k}{k_0}\right)^2 \left[\frac{k}{k_0} + \frac{k_0}{k} - \sin^2 \theta - P_\gamma P_e (1 - \cos \theta) \cos \theta \frac{(k + k_0)}{m_e} \right],$$

where θ is the photon lab scattering angle, k_0 (k) are the energies of the incident (scattered) photon, and P_γ and P_e are the polarizations of the photon and electron, respectively. For the typical luminosity at which we plan to measure $\Delta\sigma^{\gamma N}(k)$ in the flux integration mode (10^5 to 10^6 photons in coherent peak), we find a typical Compton coincidence rate from

the primary coherent photon peak to be 1 event per spill. The typical analyzing power integrated over the acceptance of the polarimeter is 0.6. For typical values $P_\gamma = 0.7$ and $P_e = 0.8$, a photon polarization error of 0.03 can be obtained in about one hour, as shown in Table II.

z_{det} (m)	θ range (mr)	beam γ_{coh}/sp	k -range	C/sp	time(hr)
4.5	6-20	3×10^5	8-14	1.5	0.5
9.0	3-10	2×10^6	20-40	1.0	0.9

Table 2: For two Compton polarimeter detector z positions, the angular range accepted, the flux of coherent peak photons/spill, the optimal photon energy covered, the $e\gamma$ coincidence rate, and the time needed for a good polarization measurement.

The total singles rates impinging on the Compton polarimeter detectors have been calculated for the photon flux given in Table 2. We find less than 1 electron or positron per spill from Bethe-Heitler pair production using the formulas of [22] convoluted with multiple scattering in the target, and typically 20 photons/spill from atomic Compton scattering above a threshold of 50 MeV, calculated with the above formula. The calculations take into account contributions from both coherent and incoherent bremsstrahlung. The rate of small-angle hadrons is less than 1/spill. Since the detector is segmented into many elements, there will be no significant problems from pile-up or accidentals.

For the lowest photon energies, coincidences with the second hadron detector will be used to augment the angular coverage, since the polarimeter detectors cannot be less than 4.5 m from the target.

4 Target

Several combinations of magnet and refrigerator have been considered for the target in this experiment. We have elected to use a dilution refrigerator with a high field solenoid. A target setup similar to that used in SLAC experiments E143 and E155 [23] was rejected because of the difficulty in placing the detectors sufficiently close to the active target material, and the lack of an available magnet.

The dilution refrigerator that we will use is from CERN, and is presently being refurbished at the University of Virginia. This is a high power dilution refrigerator that was used in the past in the testing of polarized target materials and so has a relatively quick turn around for target sample changes. The target material will be polarized using dynamical nuclear polarization from high frequency microwaves in a field of about 5 T. At higher fields, the insufficient microwave power is available to obtain high ND_3 polarization values. The magnet coils are large enough so that all particles leaving the target at angles less than 20 degrees reach the detectors without hitting coils or other thick materials. The warm bore magnet design allows for fields up to 7 T with no additional cost, permitting considerable flexibility in planning extensions to the present proposal, or for other experiments at SLAC with solid polarized targets.

During E143/E155, NH_3 and ND_3 were polarized to 95% and 42% respectively. Recently, collaboration members polarized ND_3 to 50% after 'tempering' the sample. For best results the ammonia samples (ND_3 in particular) need secondary irradiation at helium temperatures, which we should be able to accomplish with the primary electron beam going directly into the target, if samples already irradiated in experiments at other labs are not available (although we expect they will be). Because there is essentially no heating or radiation damage from the photon beam, high polarization values averaging over 90% for the proton target and 50% for the deuteron target should be readily sustained over the lifetime of the experiment. This is in contrast to the previous experiments with an electron beam, where radiation damage resulted in lower average polarizations, and significant overhead time for annealing the targets.

The target length will be 3 cm, with a diameter of 1 cm. This corresponds to 1.8 gm/cm² of material, or 1.2 nucleons/barn. The dilution factor f (fraction of nucleons which can be polarized) will be about 0.15 (0.25) for the NH_3 (ND_3) target, assuming that 60% of the target cup contains NH_3/ND_3 , with the remaining volume filled with He. Because nuclear shadowing reduces the effective total cross section per nucleon for heavy nuclei approximately as $A^{-0.1}$ [12], the effective dilution factor f' will be improved, to about 0.18 and 0.30 for NH_3 and ND_3 , respectively. The NH_3 and ND_3 targets are about 0.04 r.l. in thickness, so that approximately 4% of the incident photons will convert to electron/positron pairs.

In order to accurately determine the A -dependence from the various nuclei in the polarized target, a small amount of beam time will be used to measure the rates from auxiliary targets consisting primarily of helium, carbon, aluminum, and copper. These targets will also allow a measurement of the dilution factor for the polarized targets.

5 Detector and Electronics

The detector package consists of two 80-layer total energy lead-scintillator calorimeters. A layout is shown in Fig. 7. The Large- θ calorimeter measures particles between 5 and 20 degrees, while the Small- θ calorimeter measures particles below 5 degrees. Each calorimeter has a total of 80 layers of 6 mm (1 r.l.) of lead alternating with 3-mm-thick layers of plastic scintillator strips. The strip orientation alternates from horizontal to vertical to provide both x and y information on the showers. The readout uses longitudinal wave-shifter bars to read out the detector in two longitudinal segments. The front (EM) segment sums the first 27 r.l. to contain the electromagnetic energy, while the back (HAD) segment sums the remaining 53 layers to measure the total hadronic energy.

Each scintillator plane is made up of forty strips each about 2 cm wide. The outer strips cover the full size of the detector and have wave-shifter bars at each end. The middle strips are of variable length to define a longitudinal conical surface corresponding to the minimum detection angle (see Fig. 7). The outer ends of these strips are also summed by wave-shifter bars. Each wave-shifter bar has a PMT at the down-beam end. A total of 640 PMTs will be needed (2 calorimeters with EM/HAD segmentation, vertical and horizontal readout, and 40 strips with readout at each end). The Large- θ calorimeter will be at a fixed

distance from the target, while the Small- θ calorimeter will be able to move along the beam axis to define a minimum scattering angle of $10\sqrt{40/k_0}$ mr. This will allow the Compton Polarimeter acceptance to be matched to the photon beam energy.

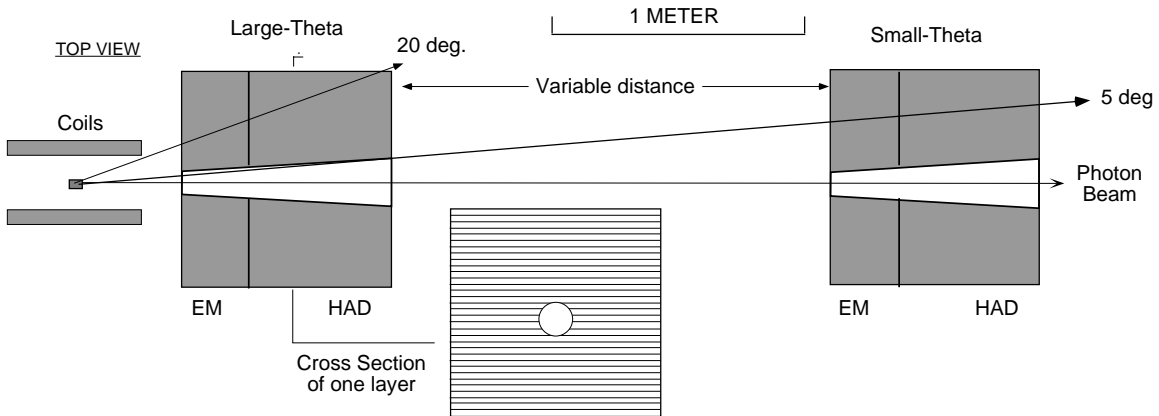


Figure 7: Two views of the proposed detector package in relation to the polarized target.

We plan to read out the PMT's using the same set of discriminators and multi-hit TDC's as used in E155. Each PMT will go to three levels of discriminator, then to a multi-hit TDC with 0.5 ns time bins. These effectively form a flash ADC system, allowing reasonably accurate measurements of the arrival time and pulse height of every event with about 11 ns dead time, in the counting mode. This technique has been successfully tested in E155 for the readout of arrays of 200 lead glass blocks detecting over 20 energetic particles per beam spill. The output of each PMT will also go to an ADC. The ADC information will be used for gain matching at low rates, and for determining the total hadronic energy in the flux integration mode.

6 Identification of Hadronic Interactions in the Presence of Electromagnetic Backgrounds

6.1 Hadronic Interactions

A hadronic interaction is characterized by one or more produced hadrons in the final state. We have used the PYTHIA Monte Carlo [25] to generate a large sample of hadronic interactions over the proposed energy range. With over 99.5% (99%) probability, at least one of these hadrons will have a transverse momentum $p_T > 0.05$ GeV ($p_T > 0.1$ GeV). Quite often, the final state will include one or more π^0 mesons, which will be detected as photon pairs, generally with a transverse momentum p_T greater than 0.1 GeV. Occasionally the hadronic final state also includes electrons or positrons from π^0 Dalitz decays or from K^0 decays.

As discussed in more detail below, the easiest way to reject electromagnetic backgrounds in the counting mode is to use a detector system that provides a good measure of the total

energy and angle of each particle (hence p_T), and distinguishes photons/electrons from hadrons by the longitudinal shower development. In the counting mode, a hadronic final state is then identified with $> 99.5\%$ efficiency by requiring at least one particle with $p_T > 0.1$, or with $p_T^H > 0.05$, where the superscript H refers to transverse momentum in the hadronic portion of the calorimeter.

The Monte Carlo events allow us to determine the idealized detector efficiency as a function of the maximum and minimum detection angles θ_{min} and θ_{max} , and the minimum energy of the particles E_{min} , with and without the detection of photons/electrons. Ideally, one would have full angular acceptance for the detectors, but in practice this is exceedingly difficult, and in fact not needed because of the forward boost from center of mass (c.m.) to lab system, which increases with energy. The previous SLAC experiment [12] found that over 99% hadronic efficiency could be obtained with $\theta_{min} = 0.4/k_0$ (where θ_{min} is in radians and k_0 in GeV is the photon energy of interest). Our studies with PYTHIA confirm this. We propose to use $\theta_{min} = 0.010\sqrt{40/k}$, which ensures $\theta_{min} < 0.01/k_0$, and cuts out $< 1\%$ of the events. The lost events are typical diffractive events, very similar to the events that are detected, so their loss should have a small (of order 1%) effect on our measured asymmetry.

For the flux integration mode, we will analyze the data in two methods: a) the first method will include all energy measured in the calorimeters (including both the electromagnetic and hadronic portions), with a calculated correction for the well-understood electromagnetic background rates and asymmetries; b) The second method of analyzing the flux integration data will be to include only the energy in the hadronic portion of the calorimeters, so that the energy from π^0 's will not be counted, but no correction for electromagnetic backgrounds will be needed. As can be seen in Fig. 8b, about 75% of the average fractional energy of hadronic events emerges in the form of charged pions, nucleons/anti-nucleons, and kaons, which will all deposit significant energy in the hadronic portion of the calorimeters. About 25% goes to photons and electrons. A few percent goes to neutrinos, whose energy is not detected at all, and about 1% goes to muons, whose energy is only partially detected. The neutrinos and muons originate from pion and kaon decays. The net result is a wide distribution in the energy deposited in the hadronic portion of the calorimeters, with a mean value exceeding 50%, and a probability of no energy being detected of less than 3% for photon energies above 10 GeV, increasing to 15% at 6 GeV (see dashed curve, Fig. 8a).

For both flux integration methods, it is desirable to have θ_{max} as large as possible, to obtain a large fraction of the total hadronic energy. The desired value of θ_{max} increases with decreasing beam energy, ultimately limiting the lowest energy at which we will be able to make good measurements. We have found that $\theta_{max} = 20$ degrees is a reasonable compromise between this desire and practical considerations of the target solenoid bore size and the detector array size. In practice, the maximum angle is slightly larger for low momentum particles due to the focusing action of the solenoidal field.

The final parameter of interest is E_{min} . In the counting mode, we find a setting of $E_{min} = 0.6 \ln(k_0)$ to be useful in increasing the percentage of events originating from photons at the coherent peak energy k_0 , with only a small loss of efficiency. This cut minimizes the number of events from low energy, less polarized photons. In the flux integration mode (method b), E_{min} is determined by the energy loss in the electromagnetic portion of the

calorimeter to be about 0.5 GeV.

For idealized detectors with 100% sampling and electronic efficiency, we plot the hadronic event detection efficiency in Fig. 8a for the counting mode cuts (solid line, $p_T > 0.1$ or $p_T^H > 0.05$, $E_{min} = 0.6 \ln(k_0)$ GeV). The flux integration (method a) efficiency is very similar, with the inefficiency mainly determined by the θ range measured ($0.01\sqrt{40/k_0} < \theta < 0.33$). As mentioned above, the flux integration (method b) efficiency is somewhat lower (dashed line), principally due to events where most of the energy is in the form of π^0 's. The efficiencies are well above 95% for both scenarios for $k_0 > 12$ GeV, but decrease rapidly below 5 GeV due to the θ_{max} cut. The counting mode efficiencies are higher, and have less energy dependence, than the flux integration mode (method b) efficiencies. On the other hand, the flux integration mode is most useful at high energies, where the expected value of $\Delta\sigma^{\gamma N}(k)$ is smallest. In the counting mode, we can study the sensitivity of $\Delta\sigma^{\gamma N}(k)$ to most of the cuts used, to determine systematic errors due to possible helicity-dependent kinematic shifts in the particle distributions.

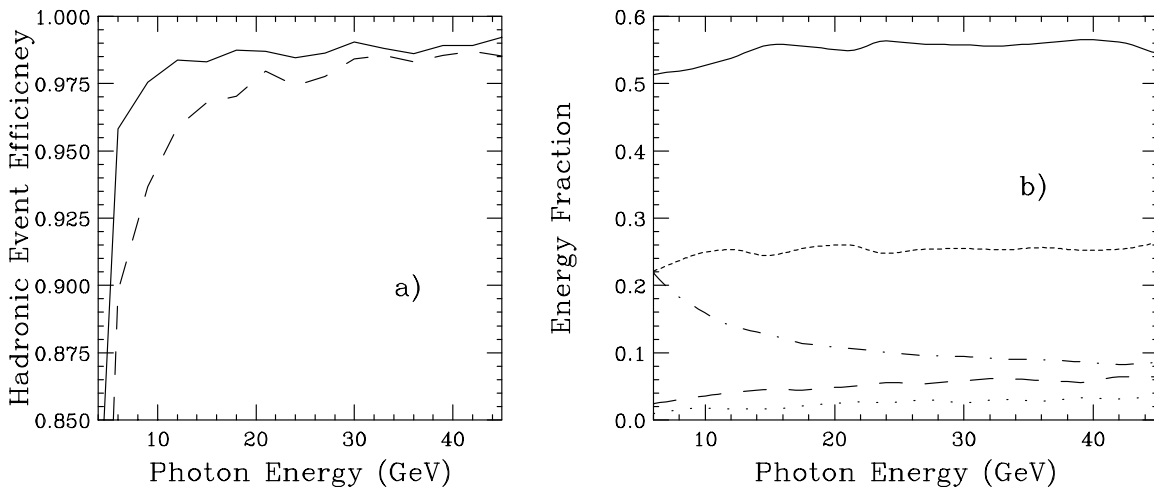


Figure 8: a) Efficiency for detecting hadronic events with the proposed detector and cuts for counting mode and flux integration method a (solid line) and flux integration mode method b (dashed curve), as defined in the text. b) Fractional energy of hadronic events that emerges in the form of charged pions (solid curve), photons/electrons (short dashed curve), nucleons/anti-nucleons (dot-dashed curve), kaons (long dashed curve), and neutrinos (dotted curve). The wiggles are due to statistical fluctuations in the simulations.

6.2 Bethe-Heitler background

The electromagnetic backgrounds that we wish to reject consist principally of Bethe-Heitler electron/positron elastic and quasi-elastic pair production [22] and Compton scattering from atomic electrons. These reactions occur at low p_T (0.0005 GeV for Bethe Heitler, $\sqrt{0.00025E}$ for atomic Compton), and always have an electron in the final state. Previous experiments [12, 8] reject electromagnetic backgrounds by rejecting tagged photons for which a forward

angle electron is detected. We instead reject electromagnetic backgrounds in the counting mode with a p_T cut of 0.1 GeV for particles identified as photons/electrons in the detector. In the flux integration mode, we can either correct for the electromagnetic background with a calculation (method a), or count only the energy in the hadronic (HAD) portions of the calorimeters (method b).

Because the target is about 0.04 r.l. and 1.2 b^{-1} in thickness, and roughly one electron/positron pair is produced per radiation length, compared to a hadronic interaction rate of 10^{-4} per b^{-1} , the Bethe-Heitler rate is about 400 times larger than the hadronic interaction rate per photon. Fortunately, most of the electron/positron pairs are produced at very small angles (characteristic angle is m_e/k).

We have calculated the total rate of Bethe-Heitler electrons (or positrons) for the Small- θ and Large- θ calorimeters as a function of minimum p_T for typical flux counting mode running conditions (3×10^4 photons per spill for each of the coherent and incoherent contributions). This corresponds to about 3 nuclear interactions per spill from coherent photons. The results are shown in Fig. 9 for a coherent peak energy of 40 GeV (the results are very similar at other energies). With no p_T cut, the rate will be several hundred low energy electrons per spill, with an average energy of about 100 MeV. Most of these will be below the detector threshold, and they simply make a tolerable “sprinkle hit” background when spread over the many scintillator paddles in each detector. The rate decreases rapidly with increasing p_T cut. Above $p_T = 0.1$, the rate (summed over both detectors) is less than 0.06/spill, mostly coming from low energy photons with no appreciable circular polarization. After subtracting incoherent contributions, the rate drops to less than 0.01/spill, or a 0.3% contamination of the hadronic events. We will correct for both the residual rate of Bethe-Heitler pairs, as well as the value of $\Delta\sigma_{BH}$ for this process using the recent calculations of [26]. These calculations predict very small asymmetries, when an average is taken over all lepton pairs, so that to first order the Bethe-Heitler background can be treated as a dilution factor. The magnitude of this dilution will be less than a percent for the counting mode, about 50% for flux integration method a, and negligible for flux integration method b.

6.3 Atomic Compton Background

Using the formula given in Section 3.3, we have calculated the total rate of photons and electrons (they are essentially the same) from atomic Compton scattering. The results are shown as a function of the minimum p_T of the particles for the front and back detectors for all incident photons in Fig. 10a, and from coherent photons only in Fig. 10b, for the same beam conditions as for the Bethe Heitler background shown in Fig. 9. The results change little for other beam energies. It can be seen that there is less difference in rates between the front and back counters, which both see on the order of several hundred low energy particles per spill. These are typically 10 to 50 MeV in energy, and so will be below the discriminator threshold of the detector, but will introduce some small fluctuations in the base line signal that are quite tolerable at the luminosities planned for the counting mode. With a p_T cut of 0.1 GeV, the atomic Compton rate becomes completely negligible (the

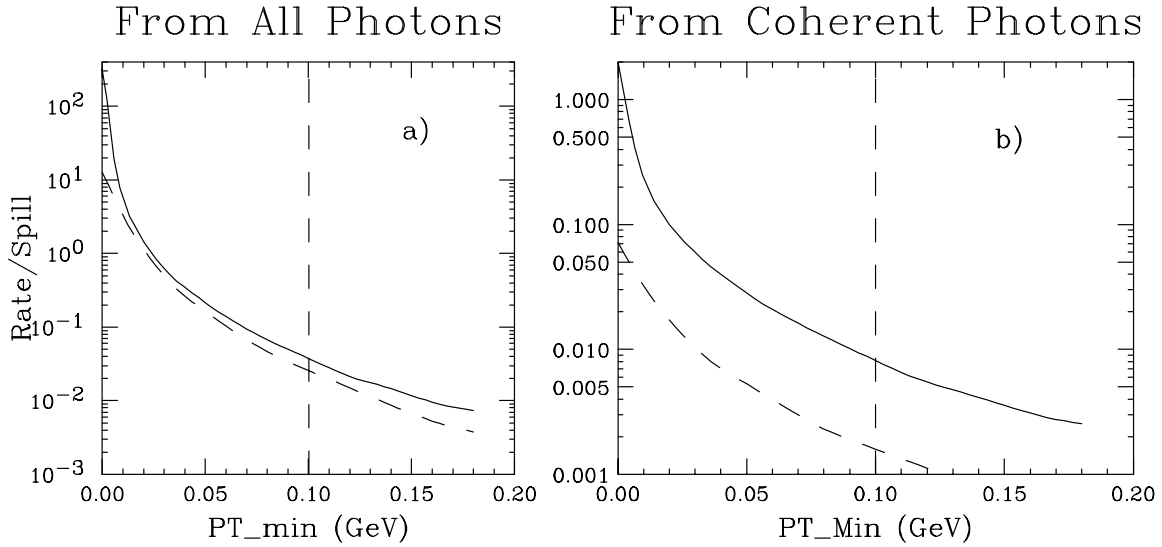


Figure 9: Rate/spill of Bethe-Heitler electrons or positrons as a function of minimum transverse momentum p_T for the front (big angle) detector (dashed curve) and back (small angle) detector (solid line) for a) all photons in the beam; b) only coherent peak photons. The beam conditions are those of Fig. 4d. The vertical dashed lines show the cut used to reject this background.

rate drops to zero beyond the kinematic limit $pT_{max} = \sqrt{m_e k/2}$, or 0.11 GeV for 48 GeV photons). In summary, the effective dilution factor from this background will be negligible for the counting mode and flux integration method b, and approximately 10% to 20% for flux integration method a.

7 Detector Rates

For the typical running conditions listed in Table I, we have calculated the total number of charged hadrons hitting the front (back) detectors to increase from about 30/spill (4/spill) for an endpoint energy of 12 GeV to about 50/spill (12/spill) for an endpoint energy of 48 GeV. The actual measured rates will be about 20% to 40% lower, since about this fraction of the hadrons will be below discriminator threshold in the detectors. Given the detector granularity, the dead time of 11 ns in the multi-hit TDC's, and the TDC time resolution of 0.5 ns, this luminosity is about the highest that we can run with 500 ns long beam pulses in the counting mode.

The total rate of soft photons and electrons has been discussed in the section above and will provide a tolerable “sprinkle hit” level in the electromagnetic segment of the calorimeter.

The most difficult background to calculate is that induced by soft neutrons. Scaling from a measurement of 2.3×10^{12} neutrons per second per kW for a totally absorbed photon beam, we estimate about 500 neutrons per spill entering the detectors for a typical

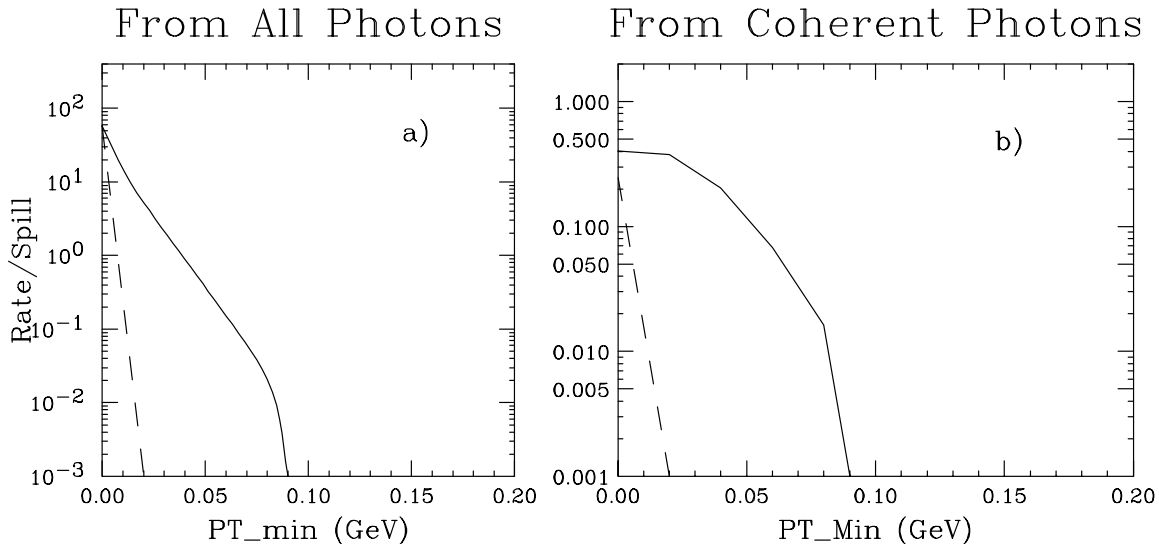


Figure 10: Rate/spill of atomic Compton electrons or photons as a function of minimum transverse momentum p_T for the front (big angle) detector (dashed curve) and back (small angle) detector (solid line) for a) all photons in the beam; b) only coherent peak photons. The beam conditions are those of Fig. 4d.

counting mode luminosity, if no beam hardener is used. We estimate this is reduced to less than 100/spill with the beam hardener, since most of these neutrons are very low energy (from excitations of the giant dipole resonance). The average energy deposited from these neutrons will rarely be above the calorimeter discriminator threshold, and so will almost never cause a signal that could be confused with an energetic hadron. In the flux integration mode, the total contribution from soft neutrons is less than 1% of the energy from hadronic showers, and will be subtracted away when the difference of rates with and without coherent photons is taken.

8 Expected results

In either the counting or flux integration technique, there are two methods to determine $\Delta\sigma^{\gamma N}(k)$. The more conservative one uses the difference in asymmetries and rates measured with and without the coherent bremsstrahlung peaks. Preliminary estimates indicate that about a factor of two smaller statistical errors can be obtained by taking advantage of the fact that the high energy incoherent photons are also longitudinally polarized, and making a simultaneous fit to all of the data.

Here we present in more detail only the results of the first method. In this case, the error on $A_1(k) = \Delta\sigma^{\gamma N}(k)/2\sigma^{\gamma N}(k)$ is given by

$$\delta A_1(k) = \frac{1}{P_\gamma P_{t,f} \sqrt{N_c}} \frac{\sqrt{2-r}}{\sqrt{r}},$$

where P_γ is the average photon polarization in the coherent peak region (typically 0.7), and P_t is the target polarization (0.9 for NH_3 , 0.5 for ND_3), The error on $\Delta\sigma^{\gamma N}(k)$ is simply obtained by scaling the error on $A_1(k)$ by $2\sigma^{\gamma N}(k)$, which is approximately constant at $250 \mu\text{b}$ in our energy range. The dilution factor f is about 0.18 (0.30) for NH_3 (ND_3). The ratio r is the fraction of all detected events originating from coherent bremsstrahlung, taking into account the detector efficiency as a function of photon energy. This will depend on the cuts used for the total measured energy of each event, as well as the minimum energy required for the most energetic particle. For cuts that preserve high overall efficiency, r ranges from 0.3 to 0.8 (see Table I), so we will take $r = 0.5$ as a typical value. For beam intensities that give $N_c = 4$ coherent bremsstrahlung events per spill (the approximate limit for flux counting mode), we find the typical error after 10^7 (4×10^7) beam spills will be $\delta A_1(k) = 0.0024$ (0.0017) for the NH_3 (ND_3) target, or $\delta\Delta\sigma^{\gamma N}(k) = 0.6$ (0.4) μb . Actual predicted errors for four coherent photon spectra are given in Table I, and are somewhat higher or lower, depending on the relative energy of the coherent peak chosen. Using the approximate relation that $A_1^n = 2A_1^d - A_1^p$, the corresponding neutron error would be $\delta A_1(k) = 0.003$, or $\delta\Delta\sigma^{\gamma n}(k) = 0.9 \mu\text{b}$.

It is difficult to make an optimized run plan in the total absence of previous measurements in the energy range of this proposal. We present a reasonable plan here based on the expectation [6, 5] that $\Delta\sigma^{\gamma N}$ for the proton (neutron) will range from about $-20 \mu\text{b}$ ($20 \mu\text{b}$) at 4 GeV to 0 ($2 \mu\text{b}$) at 40 GeV. We can also obtain an estimate from the inclusive hadron data measured in E155 [27]. In this experiment, a bremsstrahlung beam with endpoint energy of 48.5 GeV was incident on a polarized NH_3 target. Hadrons with momenta greater than 10 GeV were detected in a spectrometer centered at 2.75 degrees. Taking an average photon de-polarization factor of about 0.5, and assuming that these low p_T hadrons are somewhat representative of the total hadronic cross section, we can deduce a value of about $-2 \mu\text{b}$ for the proton target at an average photon energy around 30 GeV, and about $2 \mu\text{b}$ for a neutron target (based on the observation of a deuteron asymmetry that is consistent with zero). These results are of the same order of magnitude as the theoretical estimates [6, 5].

If in a preliminary analysis $\Delta\sigma^{\gamma N}$ turns out to be much larger than expected, more time would be devoted to optimizing systematic errors, and less on reducing statistical errors. This would be accomplished using more running time in the counting mode, and less in the flux integration mode. The following run plan is based on a total of 3×10^8 beam spills (the average amount obtained in experiments E154, E155, and E155x, each of which used 2 months of calendar time at 120 Hz). An extension to this proposal would require an additional month for the ^3He target.

We propose to take data on NH_3 in the counting mode at ten coherent peak energies ranging from 4 to 40 GeV, obtaining a statistical error of approximately $\delta\Delta\sigma^{\gamma p}(k) = 0.6 \mu\text{b}$ at each point using 10^7 beam spills. Counting mode data for the deuteron would be taken at three of these energies, with an extracted neutron error of $\delta\Delta\sigma^{\gamma n}(k) = 0.9 \mu\text{b}$ using 4×10^7 beam spills. We will then repeat all ten beam energies in the flux integration mode with both NH_3 and ND_3 targets using the remaining 10^8 beam spills. The photon beam flux will be increased by about a factor of 100 by simultaneously increasing the beam

current and reducing the beam hardener thickness. The statistical errors will be more than a factor of three smaller than for the counting mode, even after accounting for the dilution from unwanted electromagnetic background in flux integration method a.

The more conservative expected statistical errors are plotted as a function of coherent photon peak energy in Fig. 11 for the proton and neutron, for both the counting and flux integration modes. The errors are sufficiently small that a clear determination of the energy dependence of $\Delta\sigma^{\gamma N}(k)$ will be possible, judging by the range of theoretical estimates shown on the plots. The systematic error will likely be dominated by overall scale errors on beam polarization, target polarization, and target dilution factor, with additional uncertainties from the detailed shape of the coherent bremsstrahlung. Based on previous experience in E154/E155, we estimate these combined effects to be 6% to 8% of the measured results, or 0.1 to 1.5 μb . Additional systematic errors for the flux integration mode due to uncertainties in the electromagnetic background (for method a), or helicity-dependent energy fraction into π^0 's (method b), are estimated to contribute between 0.5 and 1 μb . Much more accurate systematic error estimates will be possible once all the data is taken and analyzed.

As mentioned above, smaller counting mode statistical errors will be obtained in an alternate analysis using a simultaneous fit to all of the data, including the events from the high energy incoherent photons. This procedure is similar to the iterative radiative correction procedure needed in deep inelastic electron scattering, with which we have extensive experience. It will be simplified by only having one relevant kinematic variable (photon energy), rather than two (x and Q^2).

The granularity of the detector will allow several systematic checks to be performed, such as checking that varying θ_{min} , θ_{max} , or E_{min} within reasonable ranges has no effect on the measured asymmetry. We plan to check for possible rate dependent effects by running at several beam currents at one energy.

As in previous experiments, most false asymmetries will be canceled by random pulse-to-pulse helicity flips of the electron beam, well as frequent reversals of the target polarization direction.

9 Request

We request two weeks running time at low repetition rate to check out the photon beam, target, and detectors. We request two months of production running at 120 Hz, to be divided approximately equally between low current (counting mode) and high current (flux integration) for the electron beam. Assuming a slightly lower efficiency than E155/E155x due to concurrent running with the B factory, combined with overhead for energy and target changes, beam polarization measurements, and other systematic checks, two calendar months should be enough to obtain the 3×10^8 beam spills (30 perfect days) of production running used in our run plan.

We request the re-establishment of the polarized photon beam capability as used in E78. This will involve re-installation of the goniometer, refurbishing the dump magnets, installing a new beam dump, making a photon collimator, and installation of the standard

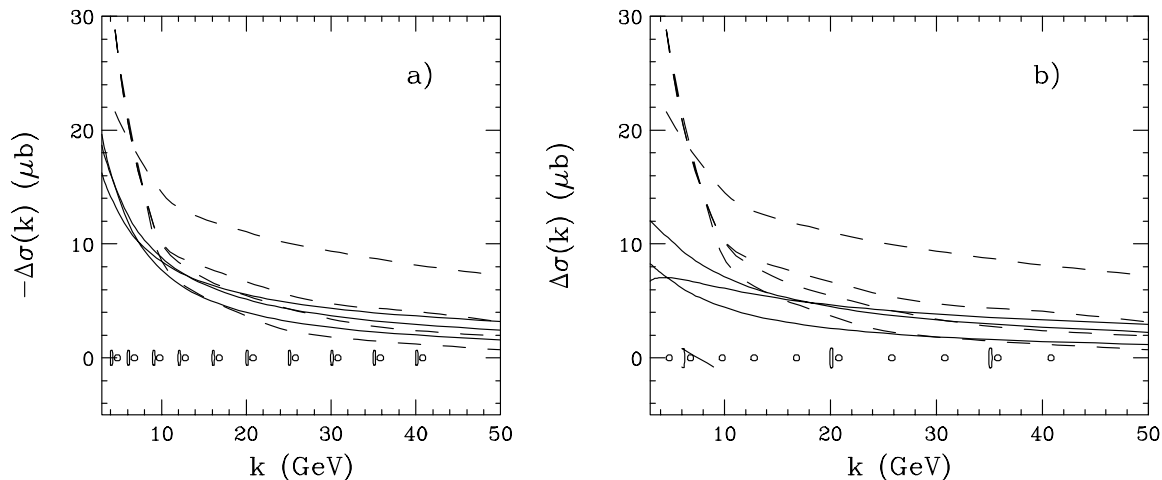


Figure 11: a) Estimated proton error bars for $\Delta\sigma^{\gamma p}(k)$ for this proposal as a function of photon energy for the counting mode (rectangles) and flux integration mode (circles). The symbol heights represent the expected statistical errors in the more conservative analysis. Systematic errors are not shown, but are expected to be 6% to 8% of the measured values of $\Delta\sigma^{\gamma N}(k)$. The dashed curves are representative models from [6], the solid curves are from [5]; b) same but for the neutron as measured with ND_3 .

photon beam monitors. The components of the Compton polarimeter exist at SLAC; the collaboration will cut lead glass blocks used as detectors to the desired size.

Concerning the three diamonds owned by SLAC, we would like to have the two thicker diamond crystals thinned down to the same thickness as the thin crystal (0.0007 r.l.), to be used as spares. Additional diamonds will be supplied by the collaboration (Yerevan group).

The collaboration will furnish most of the equipment needed for the target, such as the dilution refrigerator, pumps, microwave tubes, NMR equipment, and target material. The principal request is from SLAC is for the target magnet, which is based on an existing design.

We will need resources to acquire the scintillator strips and wave-shifter bars for the two large calorimeters. The two detectors combined require approximately 640 PMTs, and 1920 channels of discriminator and TDC. An approximate increase of 20% in the existing inventory in E.S.A. will be sufficient to meet these needs. In addition, 640 channels of ADC will be needed.

Members of the collaboration have experience with all of the equipment used in this experiment, and have successfully carried out similar experiments with virtual photons.

References

- [1] S. D. Drell and A. C. Hearn, Phys. Rev. Lett. 16, 908 (1966); S. B. Gerasimov, Yad. Fiz. 2, 598 (1966); S.J. Brodsky and J.R. Primack, Ann. Phys. 52 (1969) 315.

- [2] L. Tiator, D. Drechsel, and S.S. Kamalov, <http://arXiv.org/abs/nucl-th/000561> and references therein; <http://arXiv.org/abs/hep-ph/0008306>.
- [3] J. D. Bjorken, Phys. Rev. 148 (1966) 1467; Phys. Rev. D 1 (1970) 1376.
- [4] I. Karliner, Phys. Rev. D7 (1993) 2717; R.L. Workman and R.A. Randt, Phys. Rev. D45 (1992) 1789; A.M. Sandorfi, C.S. Whisnant, and M. Khandaker, Phys. Rev. D50 (1994) R6681; R.A. Randt, I.I. Strakovsky, R.L. Workman, Phys. Rev. C53 (1996) 440; D. Drechsel, G. Klein, Phys. Rev. D58 (1998) 116609.
- [5] N. Bianchi, E. Thomas, Phys. Lett. B 450 (1999) 439; E. Thomas, N. Bianchi, Nucl. Phys. Proc. Suppl. 82 (2000) 256.
- [6] S.D. Bass and M.M. Brisudova, Eur. Phys. J. A4 (1999) 251; S.D. Bass, Mod. Phys. Lett. A12 (1997) 1051 and references therein.
- [7] P.V. Landshoff and S.D. Bass, Phys. Lett. B336 (1994) 537; Close and Roberts, Phys. Lett. B336 (1994) 257.
- [8] For a review, see talks from each laboratory presented at the GDH2000 conference, June 2000, Mainz, Germany. Proceedings to be published by World Scientific (ed. Dieter Drechsel).
- [9] H. Arenhovel, nucl-th/0006083 (GDH2000 conference, June 2000, Mainz, Germany).
- [10] F. M. Steffens *et al.*, Phys. Lett. B447 (1999) 233.
- [11] SLAC E155, P.L. Anthony *et al.*, Phys. Lett. B463 (1999) 339; O. A. Rondon, Phys. Rev. C60 (1999) 035201.
- [12] D.O. Caldwell *et al.*, Phys. Rev. D7 (1973) 1362.
- [13] W. Kaune *et al.*, Phys. Rev. D 11, 478 (1975).
- [14] R. Schwitters, SLAC-TN-70-32 (1970).
- [15] G. Miller and D. Walz, SLAC-PUB-1297.
- [16] D. Luckey and R. Schwitters, Nucl. Instrum. Meth. 81, 164 (1970).
- [17] G. Diambri Palazzi, Rev. Mod. Phys. 40, 611 (1968).
- [18] R. Jones, <http://zeus.phys.uconn.edu/halld/cobrems-7-97/>
- [19] R. F. Mozley and J. DeWire, Nuovo Cimento 27, 1281 (1983).
- [20] I. M. Nadzhafov, Bulletin of the Academy of Sciences of the USSR, Physical Series Vol 14, No. 10, p. 2248 (1976).
- [21] H. A. Tolhoek, Rev. Mod. Phys. 28 (1956) 277.

- [22] Y.S. Tsai, Rev. Mod. Phys. 46 (1974) 815; 49 (1977) 421 (E).
- [23] T.D. Averett *et al.*, Nucl. Instrum. Meth.A 427 (1999) 440.
- [24] SLAC E154, K. Abe *et al.*, Phys. Rev. Lett. 79 (1997) 26.
- [25] T. Sjostrand, Computer Physics Commun. 82, 74 (1994).
- [26] T. Gehrman, M. Stratmann, Phys. Rev. D56 (1997) 5839.
- [27] E155 Collaboration, P.L. Anthony *et al.*, Phys. Lett. B458 (1999) 536.